Advances in Nano Research, *Vol. 16, No. 4 (2024) 413-426*
https://doi.org/10.12989/anr.2024.16.4.413

Free and forced vibration analysis of FG-CNTRC viscoelastic plate using high shear deformation theory

Mehmet Bugra Özbey[1], Yavuz Cetin Cuma[1], İbrahim Ozgur Deneme[2] and Faruk Firat Calim*[1]

[1]*Department of Civil Engineering, Adana Alparslan Turkes Science and Technology University, Adana, Türkiye*
[2]*Department of Civil Engineering, Aksaray University, Aksaray, Türkiye*

(*Received January 6, 2024, Revised February 20, 2024, Accepted February 29, 2024*)

Abstract. This paper investigates the dynamic behavior of a simply supported viscoelastic plate made of functionally graded carbon nanotube reinforced composite under dynamic loading. Carbon nanotubes are distributed in 5 different shapes: U, V, A, O and X, depending on the shape they form through the thickness of the plate. The displacement fields are derived in the Laplace domain using a higher-order shear deformation theory. Equations of motion are obtained through the application of the energy method and Hamilton's principle. The resulting equations of motion are solved using Navier's method. Transforming the Laplace domain displacements into the time domain involves Durbin's modified inverse Laplace transform. To validate the accuracy of the developed algorithm, a free vibration analysis is conducted for simply supported plate made of functionally graded carbon nanotube reinforced composite and compared against existing literature. Subsequently, a parametric forced vibration analysis considers the influence of various parameters: volume fractions of carbon nanotubes, their distributions, and ratios of instantaneous value to retardation time in the relaxation function, using a linear standard viscoelastic model. In the forced vibration analysis, the dynamic distributed load applied to functionally graded carbon nanotube reinforced composite viscoelastic plate is obtained in terms of double trigonometric series. The study culminates in an examination of maximum displacement, exploring the effects of different carbon nanotube distributions, volume fractions, and ratios of instantaneous value to retardation times in the relaxation function on the amplitudes of maximum displacements.

Keywords: carbon nanotube reinforced composite (CNTRC); forced vibration analysis; higher-order shear deformation theory; Laplace transform; linear standard viscoelastic model; plate

1. Introduction

Carbon nanotubes have an important role in engineering areas due to their mechanical properties such as high strength and low weight. The employment of carbon nanotubes in composite materials have been an active area of research for quite some time. Thostenson *et al*. (2001) conducted a study on examining the mechanical properties and modelling carbon nanotubes. Cadek *et al*. (2002) observed the effect of hardness and Young's modulus, which are characteristics of carbon nanotube, on the fundamental frequency values. Temel *et al*. (2004) carried out study on the dynamic behavior of viscoelastic helices. Fiedler *et al*. (2006) conducted a study on the material properties and mechanical properties of carbon nanotubes. Zhu *et al*. (2012), Lei *et al*. (2013), Lin and Xiang (2014) and Alibeigloo and Emtehani (2015) performed a free vibration analysis for carbon nanotubes using different energy method and examined the effects of various carbon nanotube distributions and geometric properties on the analysis. Duc and Quan (2014) performed forced vibration analysis for functionally graded material (FGM) shell and observed the effects of material, geometric and foundation properties on the analysis. Mirzaei and Kiani (2015) studied the temperature-dependent buckling of carbon nanotube reinforced sandwich plate. Kim (2015), represent the foundation in functionally graded material (FGM) cylindrical shells partially resting on the elastic foundation with Pasternak model and performed a free vibration analysis. Ansari *et al*. (2015) carried out a forced vibration analysis for carbon nanotube reinforced composite (CNTRC) plate. First order shear deformation theory (FSDT) was used to obtain the displacement fields and the solution of the equations of motion was carried out by Galerkin method. They examined the effects of different carbon nanotube distributions and carbon nanotube volume coefficients on forced vibration analysis. Malekzadeh and Heydarpour (2015) investigated the effects of layering of CNTRC plates on free and forced vibration analysis. Phung-Van *et al*. (2015) used higher order shear deformation theory (HSDT) to obtain the displacements in the dynamic analysis performed for CNTRC plates. Mirzaei and Kiani (2016) examined the effect of whether CNTRC plates contain a cutout or not on free vibration analysis. Bennoun *et al*. (2016) obtained the equations of motion using Hamilton principle and examined the results of free vibration analysis of FGM sandwich plates. Mahapatra *et al*. (2016) created the equations of motion using Hamilton principle and solved using the direct iterative method. Huang *et al*. (2016) realized free vibration analysis, and in this analysis, CNTRC plate was examined layer by layer and the displacements were determined by a simple four-variable FSDT. Wang *et al*. (2016) used the classical plate

*Corresponding author, Professor,
E-mail: ffcalim@atu.edu.tr

ISSN: 2287-237X (Print), 2287-2388 (Online)

theory for CNTRC thin plate and investigated the influences of different boundary conditions of free vibration analysis. Kiani (2017) performed buckling analysis for FG-CNTRC plate subjected to parabolic loading. Ebrahimi and Habibi (2017) examined the impact response of FG-CNTRC plate by changing the material properties of CNT and matrix according to temperature. Kiani (2017) examined the effects of various boundary conditions and carbon nanotube distributions on the dynamic analysis of the FG-CNTRC cylindrical panel subjected to a moving load. Ebrahimi and Farazmandnia (2017) examined the effect of temperature-dependent material properties on free vibration analysis using the higher-order shear deformation theory. Kiani (2017) solved the equations of motion obtained by Hamilton's principle using Ritz method and examined the effect of CNTRC on the free vibration of spherical panels. Ansari *et al.* (2017) investigated CNTRC plate with elliptical shape. Hajmohammad *et al.* (2017) examined carbon nanotubes with Kelvin-Voigt viscoelastic model. They used *X* type carbon nanotube distribution and sinusoidal shear deformation theory as shear deformation theory. Kiani (2017) studied the effect of carbon nanotube reinforced composites on the forced vibration analysis of conical panel subjected to the impact of a moving load. Wang *et al.* (2017) investigated the effects of different boundary conditions and geometric properties on vibration analysis using coding written in MATLAB. Kiani (2019) studied the effects of different boundary conditions, carbon nanotube distributions, geometric parameters and temperature on the buckling of CNTRC beams. Truong-Thi *et al.* (2020) realized free vibration analysis by separating the tree-node triangular elements using a uniform carbon nanotube distribution. Wang *et al.* (2018) studied layering and foundation effects for CNTRC plates. Boutaleb *et al.* (2019) performed dynamic analysis for functionally graded nanoplates using higher order shear deformation theory to obtain displacement fields. Emdadi *et al.* (2019) used FSDT to determine the displacement fields in free vibration analysis for FG-CNTRC porous sandwich plate and obtained the equations motion by Ritz method. Bendaho *et al.* (2019) solved the equations of motion obtained by Hamilton's principle by Navier's method. They performed free vibration analysis for nanoplate and investigated the effects of different shear deformation theories and geometric properties on free vibration analysis. Barati *et al.* (2019) and Mirjavadi *et al.* (2022) examined the effects of different porosity distributions on the analysis. Ghasemi and Mohandes (2020), studied the effects of different geometric properties on free vibration analysis using Love's first approximation shell theory. Khosravi *et al.* (2020) solved the equations of motion obtained by Hamilton's principle by the assumed modes method. Faleh *et al.* (2020) used crystalline materials in analysis and examined the effect of the grain properties of crystalline materials on the analysis. Zannon *et al.* (2020) performed free vibration analysis by obtaining displacement fields using third-order shear deformation theory. Soleimani-Javid *et al.* (2021) performed a free vibration analysis for a sandwich plate resting on Visco-Pasternak foundation and examined the effects of various geometric and material properties and boundary conditions on free vibration analysis. Liu *et al.* (2021) examined the effects of different geometric properties, porosity coefficients and material distributions on the analysis in the forced vibration analysis. Dang *et al.* (2022) observed the effects of various porosity properties and different boundary conditions on free vibration analysis for FGM porous shells. Vinh and Tounsi (2022) carried out free vibration analysis of functionally graded porous shells with different geometric shapes. Singha *et al.* (2022) formalized the equations of motion with Langrange's equations of motion and observed the effects of shell type, temperature and various geometric properties on the free vibration analysis. Zhang *et al.* (2023) applied electric field to face sheets of functionally graded CNTRC plate and thermal loading to entire model and observed the effects of porosity, buckling load and carbon nanotube distributions on the buckling of CNTRC plate.

Following a thorough review of studies available in the literature, it can be claimed that, the number of studies regarding the forced vibration analysis of simply supported functionally graded carbon nanotube-reinforced composite (FG-CNTRC) plates are insufficient.

The present paper demonstrates the accuracy of the algorithm developed for FG-CNTRC plates by comparing free vibration analysis results with existing studies in the literature. Afterwards, parametric forced vibration analyses for the FG-CNTRC viscoelastic plates are carried out for various carbon nanotube distributions. Finally, a maximum displacement study is carried out within the scope of the parametric study. Viscoelasticity of the material is implemented by using linear standard viscoelastic model, one of the most popular viscoelastic models regarding solids. Higher order shear deformation theory (HSDT) is used to obtain the displacement field. Using Hamilton's principle, the equations of motion are obtained in Laplace domain. The results of the parametric study are translated into time domain by using Durbin's modified inverse Laplace transform algorithm.

2. Basic equations

Simply supported FG-CNTRC plate investigated in this paper is given in Fig. 1. where a is length, b is width and h is thickness of FG-CNTRC plate.

V_{CNT} is the volume fractions of carbon-nanotubes. Four different carbon nanotube distributions are examined depending on V_{CNT}. While UD (Fig. 2(a)) refers to the uniform distribution of the carbon nanotube, VD (Fig. 2(b)), OD (Fig. 2(d)), XD (Fig. 2(e)) are the distributions of the carbon nanotubes that vary according to different z dependent functions (Zhu *et al.* 2012, Malekzadeh and Heydarpour 2015, Phung-Van *et al.* 2015, Huang *et al.* 2016).

$$\begin{aligned} V_{CNT} &= V_{CNT}^{*} \quad (UD) \\ V_{CNT} &= V_{CNT}^{*}\left(1+\frac{2z}{h}\right) \quad (VD) \\ V_{CNT} &= V_{CNT}^{*}\left(1-\frac{2|z|}{h}\right) \quad (OD) \\ V_{CNT} &= V_{CNT}^{*}\left(\frac{4|z|}{h}\right) \quad (XD) \end{aligned} \tag{1}$$

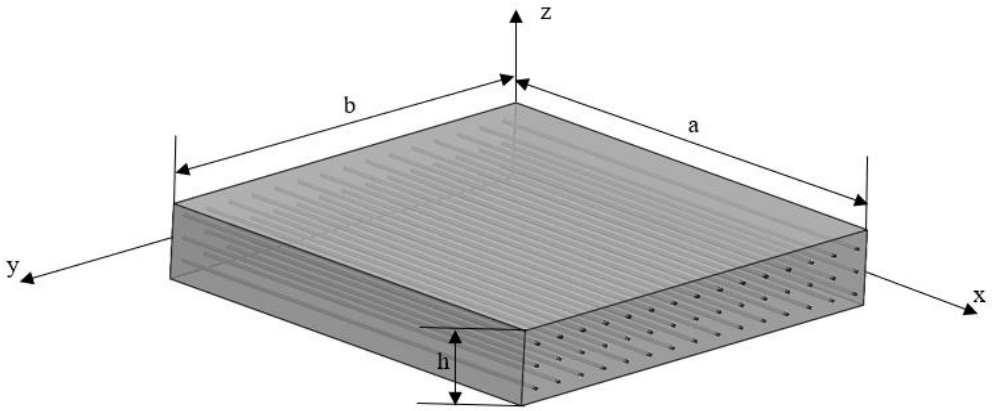

Fig. 1 FG-CNTRC plate

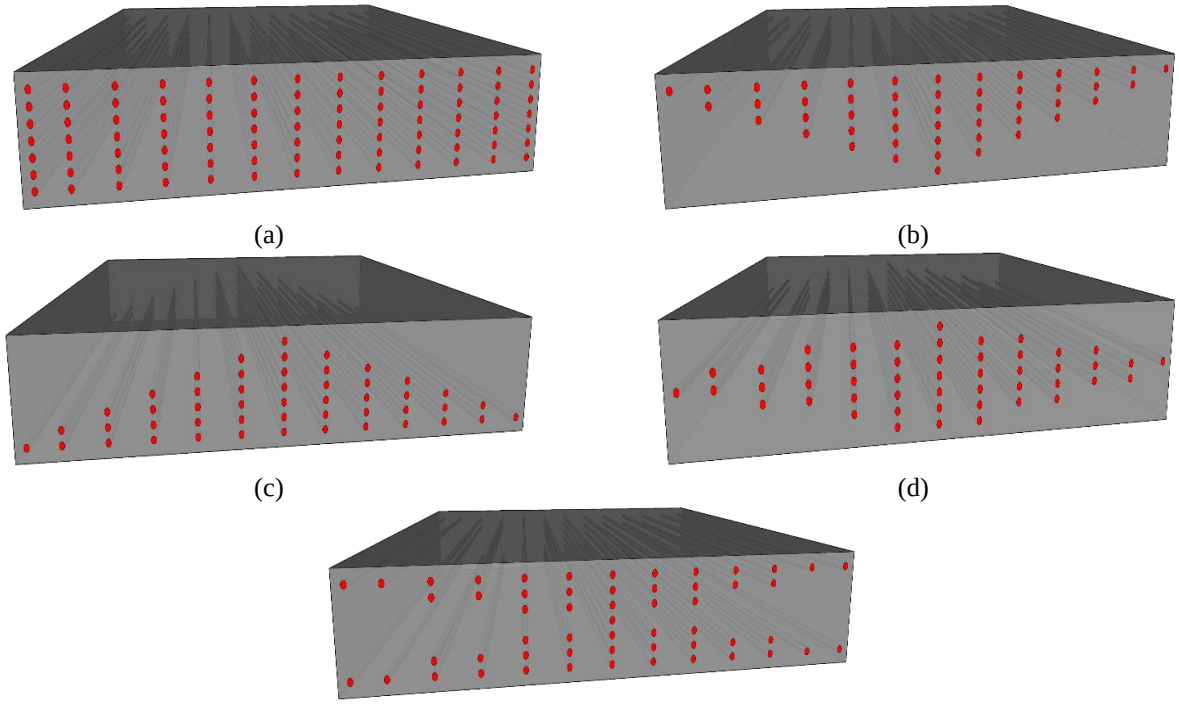

Fig. 2 Carbon nanotube distributions in FG-CNTRC plate

$$V_{CNT}^{*}=\frac{w_{CNT}}{w_{CNT}+\left(\frac{\rho^{CNT}}{\rho^{m}}\right)(1-w_{CNT})} \tag{2}$$

w_{CNT} and ρ^{CNT} represent the mass fraction and mass density of the carbon nanotube, respectively. ρ^{m} is the density of the matrix and V_{CNT}^{*} is the coefficient of carbon nanotube. The carbon nanotube distributions which can be seen in Eq. (1) are shown in Fig. 2.

The material properties of FG-CNTRC plate (Elasticity modulus E, mass density ρ, Poisson's ratio (υ) and shear modulus G) are expressed as functions of the thickness in Eq. (3).

$$\begin{aligned} E_{11}&=\eta_1 V_{CNT}E_{11}^{CNT}+V_m E^m\\ \frac{\eta_2}{E_{22}}&=\frac{V_{CNT}}{E_{22}^{CNT}}+\frac{V_m}{E^m}\\ \frac{\eta_3}{G_{12}}&=\frac{V_{CNT}}{G_{12}^{CNT}}+\frac{V_m}{G^m}\\ \upsilon_{12}&=V_{CNT}\upsilon_{12}^{CNT}+V_m\upsilon^m\\ \rho&=V_{CNT}\rho^{CNT}+V_m\rho^m \end{aligned} \tag{3}$$

where $(\,)_{CNT}$, $(\,)_m$ and η_j $(j=1,2,3)$ represent material properties of carbon nanotube and isotropic matrix and carbon nanotube efficiency coefficients. Also, V_m and G^m are volume fraction and shear modulus of matrix and are calculated as $V_m=1-V_{CNT}$ and $G^m=\frac{E^m}{2\,(1+\upsilon^m)}$, respectively.

Using HSDT, displacement fields are obtained as functions dependent on time and Cartesian coordinates (Akavci 2014).

$$u=u_o-zw_{o,x}+f(z)\,\theta_x \tag{4}$$

$$v = v_o - z w_{o,y} + f(z)\ \theta_y$$
$$w = w_o$$

Here u_o, v_o, w_o, θ_x and θ_y are displacements at the midpoint of FG-CNTRC plate in x, y and z directions and the rotation in any point of CNTRC plate around x and y axis, respectively.

$f(z)$ is the shape function of strain and stress distribution varying through thickness (Rachid *et al*. 2022, Calim and Özbey 2024, Cuma *et al*. 2024).

$$f(z) = \frac{\pi\, h}{\pi^4 + h^4} e^{\left(\frac{hz}{\pi}\right)} \left(\pi^2 sin\left(\frac{\pi z}{h}\right) + h^2 cos\left(\frac{\pi z}{h}\right)\right) - \frac{\pi\, h^3}{\pi^4 + h^4} \tag{5}$$

Strains are obtained by using the displacements obtained using Eq. (4).

$$\begin{aligned}
\varepsilon_x &= \frac{\partial u}{\partial x} = u_{0,x} - z\, w_{0,xx} + f(z)\theta_{x,x} \\
\varepsilon_y &= \frac{\partial v}{\partial y} = v_{0,y} - z\, w_{0,yy} + f(z)\theta_{y,y} \\
\gamma_{yz} &= \frac{\partial v}{\partial z} + \frac{\partial w}{\partial y} = f'(z)\theta_y \\
\gamma_{xz} &= \frac{\partial u}{\partial z} + \frac{\partial w}{\partial x} = f'(z)\theta_x \\
\gamma_{xy} &= \frac{\partial u}{\partial y} + \frac{\partial v}{\partial x} = u_{0,y} + v_{0,x} \\
&-2z\, w_{0,xy} + f(z)\,(\theta_{x,y} + \theta_{y,x})
\end{aligned} \tag{6}$$

The connection between stress and strain is as shown below (Zhu *et al*. 2012, Malekzadeh and Heydarpour 2015, Phung-Van *et al*. 2015, Huang *et al*. 2016).

$$\begin{bmatrix} \sigma_x \\ \sigma_y \\ \tau_{yz} \\ \tau_{xz} \\ \tau_{xy} \end{bmatrix} = \begin{bmatrix} Q_{11} & Q_{12} & 0 & 0 & 0 \\ Q_{21} & Q_{22} & 0 & 0 & 0 \\ 0 & 0 & Q_{44} & 0 & 0 \\ 0 & 0 & 0 & Q_{55} & 0 \\ 0 & 0 & 0 & 0 & Q_{66} \end{bmatrix} \begin{bmatrix} \varepsilon_x \\ \varepsilon_y \\ \gamma_{yz} \\ \gamma_{xz} \\ \gamma_{xy} \end{bmatrix} \tag{7}$$

Displacements are considered to be relatively small compared to the thickness of the simply supported FG-CNTRC plate. Consequently, stress and strain in the z direction can be assumed to be zero ($\sigma_z = \varepsilon_z = 0$).

The stiffness parameters (Q) can be determined using the following equations, as outlined by Huang *et al*. (2016), Malekzadeh and Heydarpour (2015), Phung-Van *et al*. (2015), and Zhu *et al*. (2012).

$$\begin{aligned}
Q_{11} &= \frac{E_{11}}{(1-\nu_{12}\nu_{21})}, \quad Q_{22} = \frac{E_{22}}{(1-\nu_{12}\nu_{21})} \\
Q_{12} &= \frac{\nu_{21}\, E_{11}}{(1-\nu_{12}\nu_{21})}, \quad Q_{44} = G_{23} \\
Q_{55} &= G_{13}, \quad Q_{66} = G_{12}
\end{aligned} \tag{8}$$

Here, ν_{21} is taken as $\frac{E_{22}}{E_{11}}$.

The force, moment and stress relationship used to obtain the equations of motion is as shown in Eq. (9).

$$\{N_x, N_y, N_{xy}\} = \int_{-\frac{h}{2}}^{\frac{h}{2}} \{\sigma_x, \sigma_y, \tau_{xy}\}\, dz \tag{9}$$

$$\{Q_x, Q_y, Q_{xy}\} = \int_{-\frac{h}{2}}^{\frac{h}{2}} f(z)\{\sigma_x, \sigma_y, \tau_{xy}\}\, dz$$
$$\{M_x, M_y, M_{xy}\} = \int_{-\frac{h}{2}}^{\frac{h}{2}} \{\sigma_x, \sigma_y, \tau_{xy}\}\, z\, dz$$
$$\{R_x, R_y\} = \int_{-h/2}^{h/2} f'(z)^2\, \{\sigma_x, \sigma_y, \tau_{xy}\}\, dz$$

Here, R, M, N, Q represent the higher order shear terms, moment resultants, plane force resultants and transverse shearing force resultants, respectively.

Hamilton's principle is used to determine the equations of motion of simply supported FG-CNTRC plate.

$$\delta \int_{t_1}^{t_2} (U - K - V) dt = 0 \tag{10}$$

U in Eq. (10) represents the strain energy of FG-CNTRC plate. Where V represents the potential energy and K represents the kinetic energy which are calculated as,

$$\begin{aligned}
U &= \int_V \left(\sigma_x \varepsilon_x + \sigma_y\, \varepsilon_y + \tau_{xy}\gamma_{xy} + \tau_{xz}\gamma_{xz} + \tau_{yz}\gamma_{yz}\right) dV \\
K &= \frac{1}{2}\int_v \rho(z)(\dot{u}^2 + \dot{v}^2 + \dot{w}^2)\, dV \\
V &= \int_A q(x,y) w\, dA
\end{aligned} \tag{11}$$

Here, ρ(z) represents the mass density function, which is dependent on the thickness of the FG-CNTRC plate. Additionally, $\dot{(\ )}$ denotes the derivative concerning time.

Variations of strain energy, potential energy, and kinetic energy are considered and substituted into Hamilton's principle, leading to the following result.

$$\int_{t_1}^{t_2} \begin{pmatrix} \int_V [\sigma_x\, \delta\varepsilon_x + \sigma_y \delta\varepsilon_y + \tau_{xy}\delta\gamma_{xy} \\ + \tau_{xz}\delta\gamma_{xz} + \tau_{yz}\delta\gamma_{yz} \\ -\rho(z)(-\ddot{u}\delta u - \ddot{v}\delta v - \ddot{w}\delta w)]dv \\ -\int_A [q(x,y)\delta w] dA \end{pmatrix} dt = 0 \tag{12}$$

The equations of motion are obtained by collecting the coefficients of the parameters δu_0, δv_0, δw_0, $\delta\theta_0$, $\delta\psi_0$ obtained from the solution of the Hamilton's principle.

$$\begin{aligned}
&-N_{x,x} - N_{xy,y} + I_1\ddot{u}_o - I_2\ddot{w}_{o,x} + I_4\ddot{\theta}_x = 0 \\
&-N_{y,y} - N_{xy,x} + I_1\ddot{v}_o - I_2\ddot{w}_{o,y} + I_4\ddot{\theta}_y = 0 \\
&-M_{x,xx} - M_{y,yy} - 2M_{xy,y,x} + I_1\ddot{w}_o + I_2\left(\ddot{u}_{o,x} + \ddot{v}_{o,y}\right) \\
&-I_3\left(\ddot{w}_{o,xx} + \ddot{w}_{o,yy}\right) + I_5\left(\ddot{\theta}_{y,y} + \ddot{\theta}_{x,x}\right) = 0 \\
&-Q_{x,x} - Q_{xy,y} + R_x + I_4\ddot{u}_o - I_5\ddot{w}_{o,x} + I_6\ddot{\theta}_x = 0 \\
&-Q_{y,y} - Q_{xy,x} + R_y + I_4\ddot{v}_o - I_5\ddot{w}_{o,y} + I_6\ddot{\theta}_y = 0
\end{aligned} \tag{13}$$

Here I_i are inertia coefficients and are calculated as follows.

$$\{I_1, I_2, I_3, I_4, I_5, I_6\} = \int_{-h/2}^{h/2} \rho(z)\{1, z, z^2, f(z), zf(z), f(z)^2\}\, dz \tag{14}$$

The force and moment expressions in Eq. (13) are obtained by using force-moment-stress-strain connections in Eqs. (6), (7) and (9).

$$\begin{gathered}
N_x = A_{11}u_{o,x} + A_{12}v_{o,y} - B_{11}w_{o,xx} - B_{12}w_{o,yy} + C_{11}\theta_{x,x} + C_{12}\theta_{y,y} \\
N_y = A_{21}u_{o,x} + A_{22}v_{o,y} - B_{21}w_{o,xx} - B_{22}w_{o,yy} + C_{21}\theta_{x,x} + C_{22}\theta_{y,y} \\
N_{xy} = A_{66}u_{o,y} + A_{66}v_{o,x} - 2B_{66}w_{o,xy} + C_{66}\theta_{x,y} + C_{66}\theta_{y,x} \\
Q_x = C_{11}u_{o,x} + C_{12}v_{o,y} - E_{11}w_{o,xx} - E_{12}w_{o,yy} + G_{11}\theta_{x,x} + G_{12}\theta_{y,y} \\
Q_y = C_{21}u_{o,x} + C_{22}v_{o,y} - E_{21}w_{o,xx} - E_{22}w_{o,yy} + G_{21}\theta_{x,x} + G_{22}\theta_{y,y} \\
Q_{xy} = C_{66}u_{o,y} + C_{66}v_{o,x} - 2E_{66}w_{o,xy} + G_{66}\theta_{x,y} + G_{66}\theta_{y,x} \\
M_x = B_{11}u_{o,x} + B_{12}v_{o,y} - D_{11}w_{o,xx} - D_{12}w_{o,yy} + E_{11}\theta_{x,x} + E_{12}\theta_{y,y} \\
M_y = B_{21}u_{o,x} + B_{22}v_{o,y} - D_{21}w_{o,xx} - D_{22}w_{o,yy} + E_{21}\theta_{x,x} + E_{22}\theta_{y,y} \\
M_{xy} = B_{66}u_{o,y} + B_{66}v_{o,x} - 2D_{66}w_{o,xy} + E_{66}\theta_{x,y} + E_{66}\theta_{y,x}
\end{gathered} \tag{15}$$

$A_{ij},\ B_{ij},\ C_{ij},\ D_{ij},\ E_{ij},\ G_{ij}$ coefficients in Eq. (15) are displacement parameters and are calculated as follows.

$$\begin{gathered}
\{A_{ij}, B_{ij}, C_{ij}, D_{ij}, E_{ij}, G_{ij}\} \\
= \int_{-h/2}^{h/2} \{1, z, f(z), z^2, zf(z), f(z)^2\}\, Q_{ij}\, dz \\
i, j = 1, 2, 6
\end{gathered} \tag{16}$$

Navier's method is used to solve the equations of motion. Fourier series used for the Navier method given below is applied to obtain the displacements.

$$\begin{aligned}
\mathrm{u_o(x,y,t)} &= \textstyle\sum_{m=1}^{\infty}\sum_{n=1}^{\infty} \mathrm{A_{mn}} \cos(\alpha x) \sin(\beta y) e^{\mathrm{iwt}} \\
v_o(x,y,t) &= \textstyle\sum_{m=1}^{\infty}\sum_{n=1}^{\infty} B_{mn}\, sin(\alpha x) \cos(\beta y)\, e^{iwt} \\
\mathrm{w_o(x,y,t)} &= \textstyle\sum_{m=1}^{\infty}\sum_{n=1}^{\infty} \mathrm{C_{mn}} \sin(\alpha x) \sin(\beta y) e^{\mathrm{iwt}} \\
\theta_x(x,y,t) &= \textstyle\sum_{m=1}^{\infty}\sum_{n=1}^{\infty} T_{xmn}\, cos(\alpha x)\, sin(\beta y) e^{iwt} \\
\theta_y(x,y,t) &= \sum_{m=1}^{\infty}\sum_{n=1}^{\infty} T_{ymn}\, sin(\alpha x)\, cos(\beta y) e^{iwt}
\end{aligned} \tag{17}$$

where α and β are $\frac{m\pi}{a}$, $\frac{n\pi}{b}$. Also, $A_{mn},\ B_{mn},\ C_{mn},$ T_{xmn} and T_{ymn} are the unknown displacement parameters that must satisfy the boundary conditions for simply supported FG-CNTRC plate. Additionally, these boundary conditions are specified in Eq. (18).

$$\begin{gathered}
u_0(x,0,t) = 0,\ u_o(x,b,t) = 0,\ v_o(0,y,t) = 0 \\
w_o(x,0,t) = 0,\ w_o(x,b,t) = 0,\ w_o(0,y,t) = 0 \\
M_y^s(x,0,t) = 0,\ M_y^s(x,b,t) = 0,\ M_x^s(0,y,t) = 0 \\
M_y^b(x,0,t) = 0,\ M_y^b(x,b,t) = 0,\ M_x^b(0,y,t) = 0 \\
\theta(x,0,t) = 0,\ \theta(x,b,t) = 0,\ \psi(0,y,t) = 0 \\
N_y(x,0,t) = 0,\ N_y(x,b,t) = 0,\ N_x(0,y,t) = 0 \\
v_o(a,y,t) = 0,\ w_o(a,y,t) = 0,\ M_x^s(a,y,t) = 0 \\
M_x^b(a,y,t) = 0,\ \psi(a,y,t) = 0,\ N_x(a,y,t) = 0
\end{gathered} \tag{18}$$

The dynamic distribution load obtained using the double trigonometric series is Eq. (19).

$$\begin{aligned}
q(x,y,t) &= \sum_{m=1}^{\infty}\sum_{n=1}^{\infty} Q_{mn}(t)\, Sin\left(\frac{m\pi x}{a}\right) Sin\left(\frac{n\pi y}{b}\right) \\
Q_{mn}(t) &= \frac{4}{ab}\int_{-a/2}^{a/2}\int_{-b/2}^{b/2} q(x,y,t)\, Sin\left(\frac{m\pi x}{a}\right) Sin\left(\frac{n\pi y}{b}\right) dydx
\end{aligned} \tag{19}$$

The Laplace transform is employed to convert time functions into algebraic functions. The Laplace transform of a time function is expressed as follows:

$$L[f(t)] = \bar{F}(p) = \int_0^{\infty} f(t) e^{-pt} dt \tag{20}$$

Here, p represents the Laplace transform parameter. The first and second derivatives of $f(t)$ over time are provided in the Laplace domain, as detailed in the works of Calim (2003, 2020), Calim and Cuma (2022, 2023), Cuma and Calim (2021a, b, 2022), and Turker *et al*. (2023).

$$\begin{aligned}
L\left[\dot{f}(t)\right] &= p\,\bar{F}(p) - f(0) \\
L\left[\ddot{f}(t)\right] &= p^2\bar{F}(p) - pf(0) - \dot{f}(0)
\end{aligned} \tag{21}$$

Since the system is considered stationary at $t = 0$, the initial conditions are taken as $f(0) = \dot{f}(0) = 0$.

The displacements derived from the Fourier series, alongside force and moment expressions, are inserted into the resulting equations of motion, given in a matrix form.

$$\left(\begin{bmatrix} k_{11} & k_{12} & k_{13} & k_{14} & k_{15} \\ . & k_{22} & k_{23} & k_{24} & k_{25} \\ . & . & k_{33} & k_{34} & k_{35} \\ . & . & . & k_{44} & k_{45} \\ . & . & . & . & k_{55} \end{bmatrix} + p^2 \begin{bmatrix} m_{11} & m_{12} & m_{13} & m_{14} & m_{15} \\ . & m_{22} & m_{23} & m_{24} & m_{25} \\ . & . & m_{33} & m_{34} & m_{35} \\ . & . & . & m_{44} & m_{45} \\ . & . & . & . & m_{55} \end{bmatrix}\right) \begin{bmatrix} \bar{A}_{mn} \\ \bar{B}_{mn} \\ \bar{C}_{mn} \\ \bar{T}_{xmn} \\ \bar{T}_{ymn} \end{bmatrix} = \begin{bmatrix} \bar{P}_x \\ \bar{P}_y \\ \bar{Q}_{mn} \\ \bar{m}_x \\ \bar{m}_y \end{bmatrix} \tag{22}$$

The expression of the equations of motion in closed form can also be presented as follows.

$$[\boldsymbol{K}_{mn} + p^2\, \boldsymbol{M}_{mn}]\, \bar{\boldsymbol{D}}_{mn} = \bar{\boldsymbol{F}}_{mn} \tag{23}$$

Here, $\bar{\mathbf{F}}_{mn}$, $\bar{\mathbf{D}}_{mn}$, $\boldsymbol{K}$ and $\boldsymbol{M}$ respectively represent the external force vector in the Laplace domain, the unknown displacement vector, the stiffness matrix, and the mass matrix. The elements constituting the K and M matrices are detailed in Appendix A.

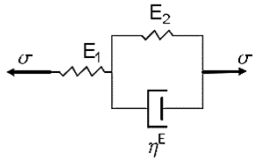

Fig. 3 Linear standard model

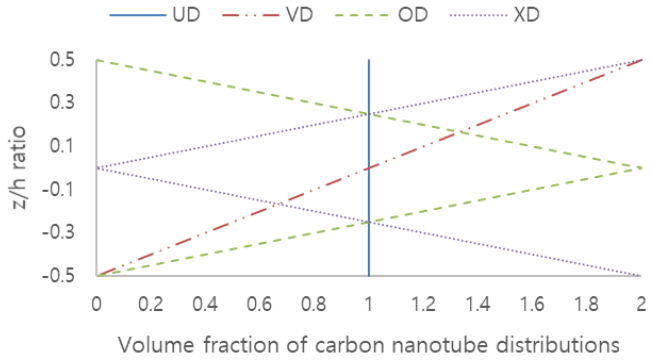

Fig. 4 Change of volume fraction throughout the thickness

Subsequently, the displacements derived from Eq. (22) need to be converted from the Laplace domain to the time domain. This transformation is achieved using Durbin's modified inverse Laplace transform procedure outlined in Appendix B. References for this transformation method include works by Durbin (1974), Narayanan (1980), Calim (2003, 2016), Cuma and Calim (2021a, b), Calim and Cuma (2022), Van Vinh and Tounsi (2022), Calim and Özbey (2023), and Cuma *et al*. (2023).

While it might be simpler to utilize elastic vibration cases in forced vibration analysis, employing viscoelastic modeling tends to yield more realistic results. For this study, the linear standard viscoelastic model, well-established for solids, is employed. Viscoelastic material properties of linear standart model can be integrated into the solution by the correspondence principle (Eratlı *et al*. 2014, Calim and Özbey 2024, Cuma *et al*. 2024). Correspondence principle depicts that the viscoelastic contants can be employed instead of elastic constants (Temel *et al*. 2004).

Linear standard viscoelastic model is shown in Fig. 3 where E_1 and E_2 are elasticity moduli for the springs used in linear standard model. η^E represents the damping coefficient of the dashpot. The viscoelastic material parameters of this model (Eratlı *et al*. 2014) can be seen in Eq. (24).

$$\bar{\mathrm{E}}_{\mathrm{v}}(\mathrm{z}) = \mathrm{E}(\mathrm{z})\left(\frac{1+\beta^{\mathrm{G}}\tau_{\mathrm{r}}^{\mathrm{G}}\mathrm{p}}{1+\tau_{\mathrm{r}}^{\mathrm{G}}\mathrm{p}}\right)$$
$$\bar{\mathrm{G}}_{\mathrm{v}}(\mathrm{z}) = \mathrm{G}(\mathrm{z})\left(\frac{1+\beta^{\mathrm{G}}\tau_{\mathrm{r}}^{\mathrm{G}}\mathrm{p}}{1+\tau_{\mathrm{r}}^{\mathrm{G}}\mathrm{p}}\right) \quad (24)$$

β^G and τ_r^G represent the ratio of instantaneous value and retardation time of the relaxation function for the linear standard model. $\bar{E}_v(\mathrm{z})$ and $\bar{G}_v(\mathrm{z})$ are the viscoelastic elasticity modulus and shear modulus, respectively. The functions for the retardation time and the instantaneous value of the relaxation function are given below,

$$\tau_{\mathrm{r}}^{\mathrm{G}} = \frac{\eta^{\mathrm{E}}}{\mathrm{E}_1+\mathrm{E}_2}$$
$$\beta^{\mathrm{G}} = (\mathrm{E}_1+\mathrm{E}_2)/\mathrm{E}_2 > 1 \quad (25)$$

3. Numerical example

This study focused on investigating the dynamic behavior of simply supported FG-CNTRC plates utilizing the linear standard viscoelastic model. An algorithm is developed using Mathematica to facilitate this analysis. To verify the accuracy of this algorithm, a free vibration analysis is conducted and compared against existing literature.

The parametric segment of the study involves a forced vibration analysis, applying a uniformly distributed impulsive step load to the plate. Initially, the investigation focus on the temporal changes in displacements concerning various carbon nanotube distributions, volume fractions, and ratios of instantaneous value (β^G) to retardation times of the relaxation function (τ_r^G). Subsequently, the study explores alterations in maximum displacements based on these parameters.

Furthermore, an additional investigation aims to depict the variation in volume fraction of carbon nanotube distributions across the plate's thickness, elucidated in Fig. 4.

3.1 Free vibration analysis of CNTRC plate

In this example, free vibration analysis is conducted for a simply supported FG-CNTRC viscoelastic plate. The fundamental frequency values obtained from this analysis are then compared with those reported in the literature by Zhu *et al*. (2012), Malekzadeh and Heydarpour (2015), Phung-Van *et al*. (2015), and Huang *et al*. (2016). Material properties for the isotropic matrix and carbon nanotube are provided in Table 1. In this study, a square plate is investigated and $a = b = 1\,m$. Also, in this example $\left(\bar{\omega} = \omega(b^2/h)\sqrt{\rho^m/E^m}\right)$ is used for non-dimensionalization. Additionally, m and n are taken as 1. The fundamental frequencies obtained from the analysis vary according to various carbon nanotube distributions (UD, VD, XD, OD), the coefficients of carbon-nanotube $(V_{CNT}^* = 0.11, 0.14, 0.17)$ and b/h ratios $\left(\frac{b}{h} = 10, 20, 50\right)$.

The results obtained from the proposed method and studies in the literature are given and compared in Table 2. It can be seen that the results obtained from the proposed method are compatible with the studies in the literature.

3.2 Forced vibration analysis of FG-CNTRC viscoelastic plate

One of the parametric studies conducted involves a forced vibration analysis of a simply supported FG-CNTRC viscoelastic plate. The plate, utilizing the material and geometric properties employed in the free vibration analysis, has a thickness of $h = 0.02m$. Additionally, m and n are taken as 1. Displacement fields are determined

Table 1 Material features used in study

$\eta_1 = 0.1490, \eta_2 = \eta_3 = 0.9340$	for $V_{CNT}^* = 0.11$
$\eta_1 = 0.1500, \eta_2 = \eta_3 = 0.9410$	for $V_{CNT}^* = 0.14$
$\eta_1 = 0.1490, \eta_2 = \eta_3 = 1.3810$	for $V_{CNT}^* = 0.17$
$E_{11}^{CNT} = 5.6466\ TPa, \quad E_{22}^{CNT} = 7.0800\ TPa$	$G_{12}^{CNT} = 1.9445\ TPa, \upsilon_{12}^{CNT} = 0.1750, \rho^{CNT} = 1400\frac{kg}{m^3}$
$E^m = 2.1000\ GPa, \upsilon^m = 0.3400, \rho^m = 1150\frac{kg}{m^3}$	$G_{13} = G_{12} = G_{23}$

Table 2 Dimensionless fundamental frequency values of simply supported FG-CNTRC viscoelastic plate

Carbon Nanotube Distributions			$V_{CNT}^* = 0.11$			$V_{CNT}^* = 0.14$			$V_{CNT}^* = 0.17$		
			b/h =10	b/h =20	b/h =50	b/h =10	b/h =20	b/h =50	b/h =10	b/h =20	b/h =50
	UD	Present	13.5680	17.3137	19.1543	14.3794	18.9093	21.3166	16.8526	21.3999	23.6066
		Zhu (2012)	13.5320	17.3550	19.2230	14.3060	18.9210	21.3540	16.8150	21.4560	23.6970
		Malekzadeh (2015)	13.4290	17.2360	19.0680	14.3030	18.8390	21.2400	16.8150	21.4560	23.6970
		Phung-Van (2015)	14.0240	17.5030	19.0930	14.9250	19.1960	21.2900	17.4090	21.6240	23.5280
		Huang (2016)	15.5500	18.2800	19.3540	16.7730	20.1820	21.5910	19.2580	22.5570	23.8440
	VD	Present	12.4642	15.0686	16.1963	13.2926	16.4892	17.9641	15.4545	18.5766	19.9101
		Zhu (2012)	12.4520	15.1100	16.2520	13.2560	16.5100	17.9950	15.4610	18.6280	19.9820
		Malekzadeh (2015)	12.2020	14.9150	16.1200	13.0060	16.3220	17.8920	15.1860	18.4230	19.8330
		Phung-Van (2015)	12.7550	15.1270	16.0930	13.6530	16.6060	17.8790	15.7880	18.6320	19.7770
		Huang (2016)	13.7530	15.5740	16.2360	14.9000	17.1810	18.0430	16.9700	19.1510	19.9380
	XD	Present	14.7236	19.9259	22.9048	15.4478	21.6134	25.5007	18.2140	24.6147	28.2750
		Zhu (2012)	14.6160	19.9390	22.9840	15.3680	21.6425	25.5550	18.2780	24.7640	28.4130
		Malekzadeh (2015)	14.6070	19.8220	22.7990	15.3370	21.5200	25.4050	18.1000	24.4990	28.1460
		Phung-Van (2015)	15.2540	20.2410	22.8800	16.1040	22.0840	25.5280	18.9690	25.0490	28.2280
		Huang (2016)	17.3620	21.4250	13.2040	18.5910	23.5980	25.9370	21.5360	26.4750	28.6190
	OD	Present	11.3214	13.3918	14.2389	12.1140	14.6592	15.7566	14.0761	16.5025	17.4735
		Zhu (2012)	11.5500	13.5230	14.3020	12.3380	14.7840	15.8010	14.2820	16.6280	17.5440
		Malekzadeh (2015)	11.7730	13.5000	14.1530	12.6620	14.8380	15.7010	14.5630	16.6250	17.3980
		Phung-Van (2015)	12.5120	13.8400	14.3000	13.5910	15.2610	15.8560	15.4290	17.0170	17.5630

using the Higher Order Shear Deformation Theory (HSDT). Equations of motion are derived through Hamilton's principle, and the solution is obtained employing Navier's method. The forced vibration analysis incorporates the linear standard viscoelastic model for damping effects.

The study explores the impact of various carbon nanotube distributions (UD, VD, XD, OD), carbon-nanotube co-efficients ($V_{CNT}^* = \{0.11,\ 0.14,\ 0.17\}$), ratios of instantaneous values ($\beta^G = 1.5, 6$), and retardation times of the relaxation function ($\tau_r^G = 0, 2\times10^{-5},\ 4\times10^{-5},\ 10\times10^{-5}$). A uniformly distributed gradual load of magnitude $10^3 \mathrm{N}/m^2$, denoted as q_0, is applied to the surface of the simply supported FG-CNTRC viscoelastic plate. The total analysis time is set to $T = 0.0512s$, utilizing 512 Laplace parameters. The obtained results for UD, VD, OD and XD carbon nanotube distributions of the FG-CNTRC plate are presented in Figs. 5-8, respectively.

The damped forced vibration analysis was performed using the linear standard viscoelastic model for a simply supported FG-CNTRC viscoelastic plate. In this analysis, a dynamic distributed load of $10^3 \mathrm{N}/m^2$ was applied to the simply supported functionally graded carbon nanotube-reinforced composite viscoelastic plate. The total solution time was set at $T = 0.0512s$ and 512, Laplace parameters were utilized for the analysis. The graphical representation of the results for the UD carbon nanotube distribution is provided in Fig. 5, showcasing displacements over time across various curves, each representing different retardation times of the relaxation function ($\tau_r^G = 0, 2\times10^{-5},\ 4\times10^{-5},\ 10\times10^{-5}$). In Fig. 5, each column represents different ratios of the instantaneous value of the relaxation function ($\beta^G = 1.5,\ 6$), while each row represents different coefficients of carbon nanotube ($V_{CNT}^* = \{0.11, 0.14, 0.17\}$).

The analysis reveals an observed increase in both the coefficient of carbon nanotube and the volume fraction of carbon nanotube, resulting in a rise in the Young's modulus (as depicted in Eq. (3)) and an overall increase in stiffness. Consequently, this leads to a decrease in displacements and periods. The increase in the ratio of the instantaneous value of the relaxation function (β^G) contributes to reduced displacements without significantly affecting the periods.

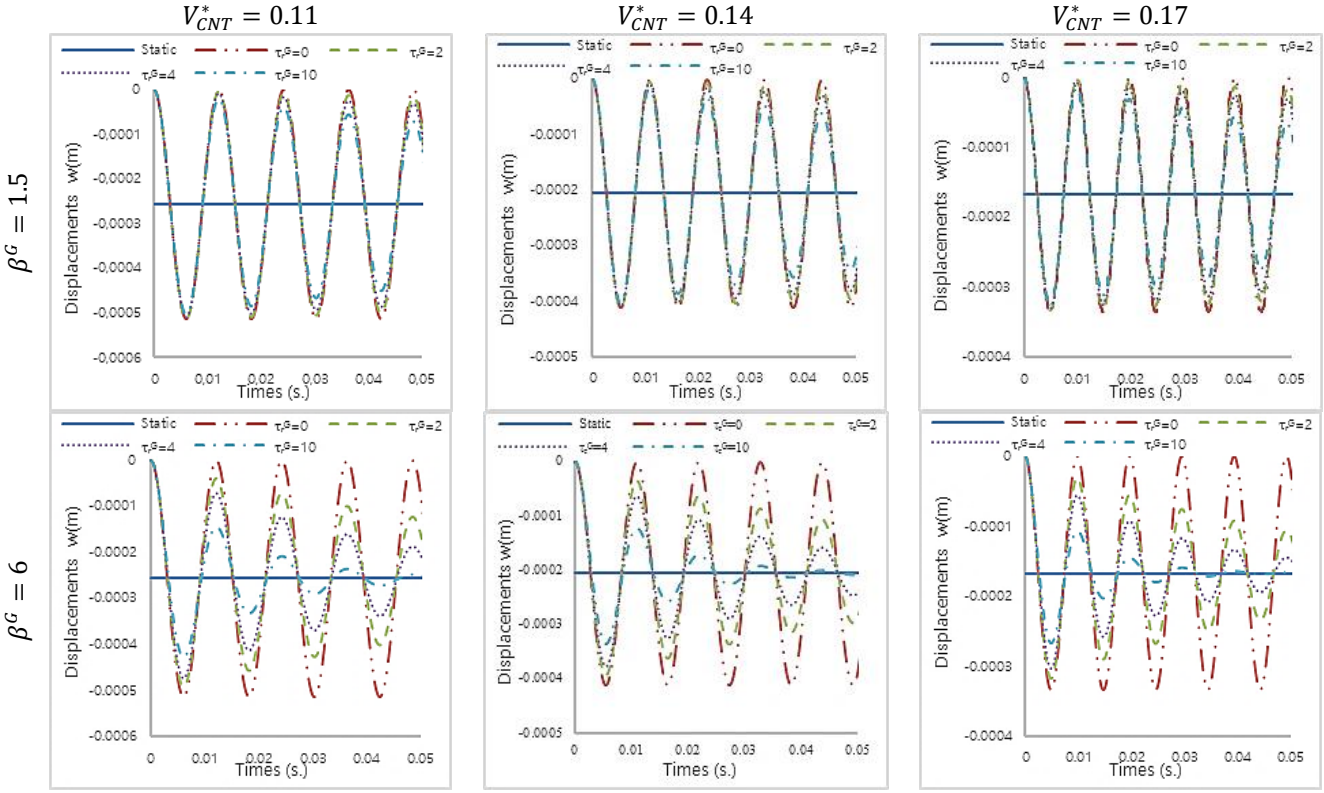

Fig. 5 Displacement at the center point of FG-CNTRC plate for UD carbon nanotube distribution $(\tau_r^G \times 10^{-5})$

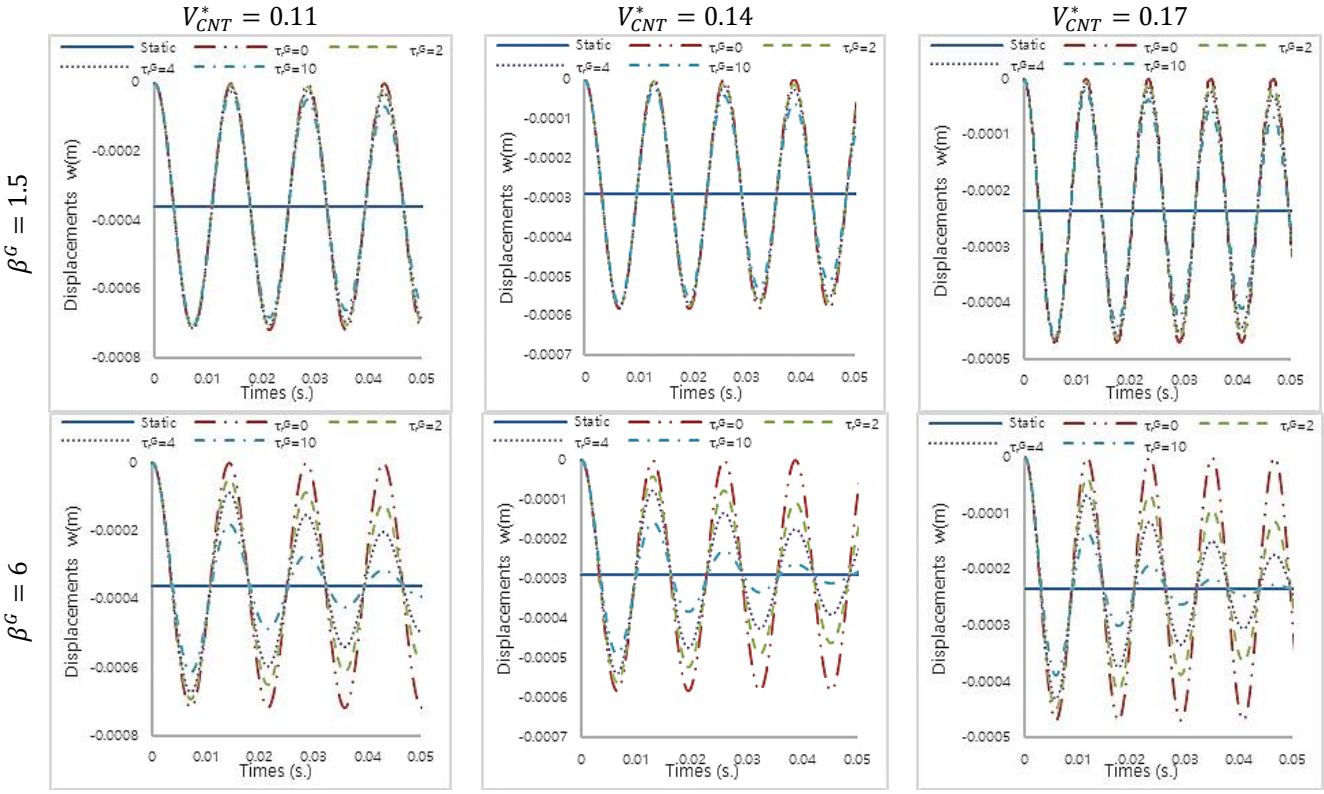

Fig. 6 Displacement at the center point of FG-CNTRC plate for VD carbon nanotube distribution $(\tau_r^G \times 10^{-5})$

Moreover, it accelerates damping. Similarly, an increase in the retardation time of the relaxation function (τ_r^G) leads to decreased displacements without a significant impact on the periods but also accelerates damping.

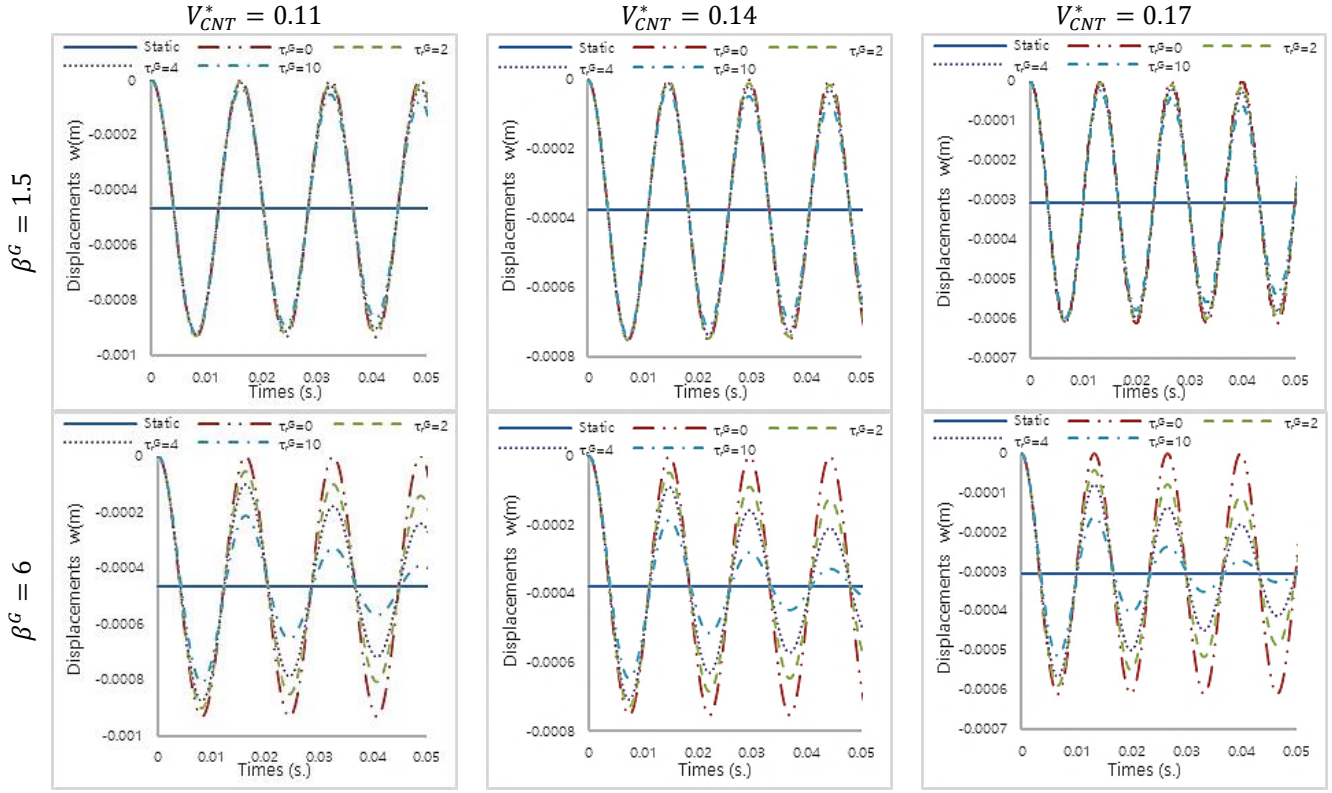

Fig. 7 Displacement at the center point of FG-CNTRC plate for OD carbon nanotube distribution $(\tau_r^G \times 10^{-5})$

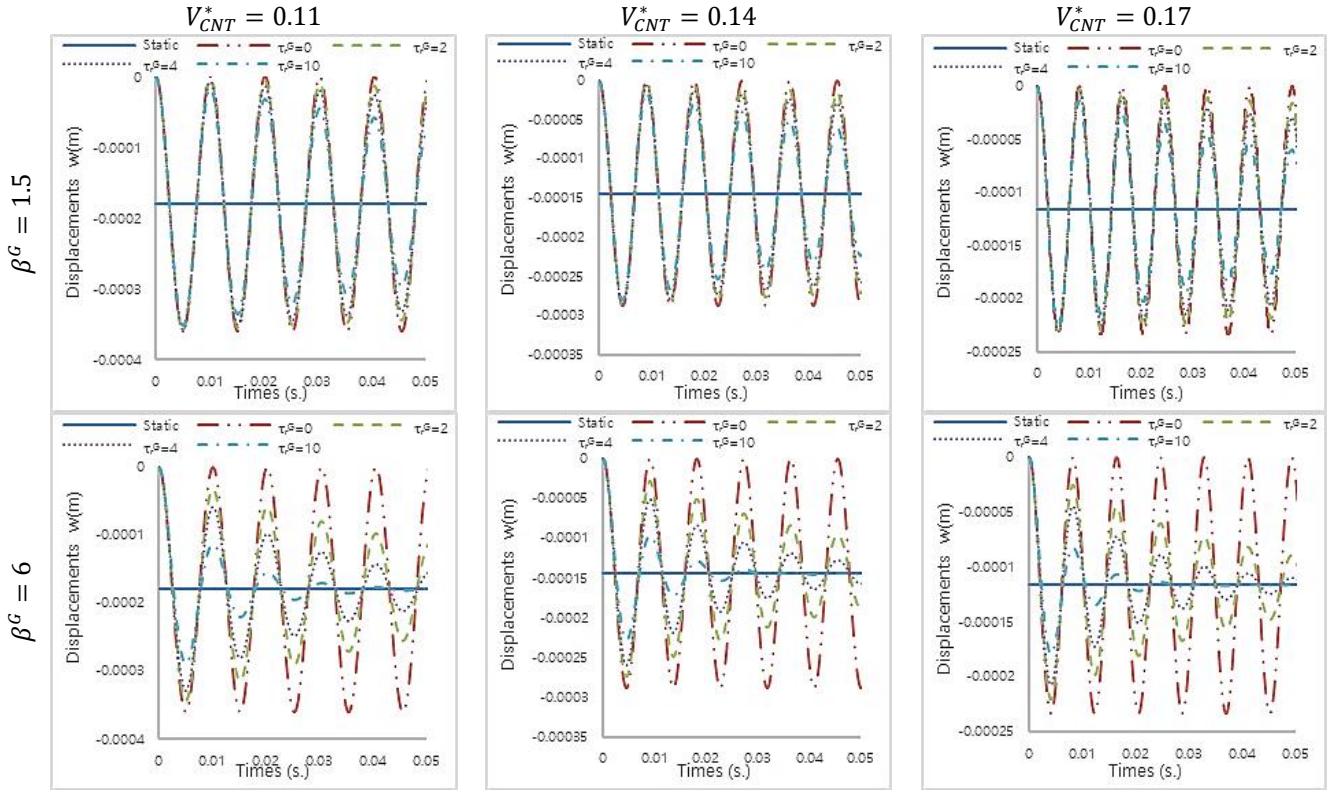

Fig. 8 Displacement at the center point of FG-CNTRC plate for XD carbon nanotube distribution $(\tau_r^G \times 10^{-5})$

Graphs demonstrating changes in displacements over time, shown in Fig. 6, are calculated for VD carbon nanotube distributions. These graphs illustrate the effects of different ratios of the instantaneous value of the relaxation

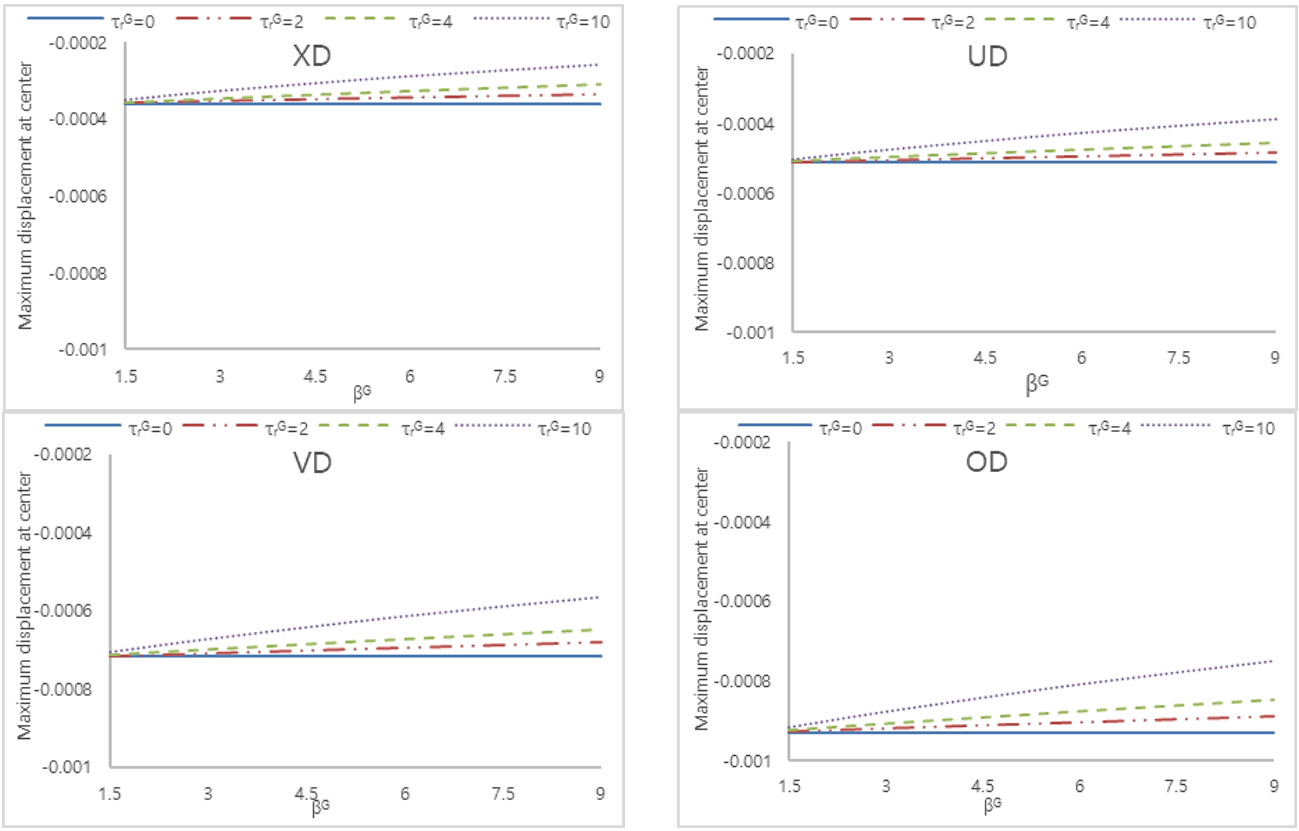

Fig. 9 Maximum displacements at the midpoints of CNTRC plate $(\tau_r^G \times 10^{-5})$

function $(\beta^G = 1.5,\ 6)$ and coefficients of carbon nanotube $(V_{CNT}^* = \{0.11,\ 0.14,\ 0.17\})$. Increases in volume fractions of carbon nanotube (V_{CNT}^*) enhance material stiffness, resulting in decreased displacements and periods under the dynamic distributed load's influence.

Figs. 7 and 8 display graphs from dynamic analyses of functionally graded carbon nanotube-reinforced composite viscoelastic plates using OD and XD carbon nanotube distributions, respectively. Similar deductions can be made for these distributions as observed in UD and VD carbon nanotube distributions. The volume fraction of carbon nanotubes affects material stiffness, with a decrease leading to increased displacements and periods. Coefficients (β^G and τ_r^G) of the linear standard viscoelastic model influence damping, contributing to decreased displacements over time without significantly affecting the periods.

Comparative analysis among UD, VD, OD and XD carbon nanotube distributions using Figs. 5 and 8 demonstrates their impact on displacements $(w_{OD},\ w_{VD},\ w_{UD},\ w_{XD})$ and periods $(P_{OD},\ P_{VD},\ P_{UD},\ P_{XD})$. The effects of the ratios of the instantaneous value and retardation time of the relaxation function, and the volume fraction of carbon nanotube, exhibit similarities across UD, VD, OD, and XD carbon nanotube distributions, albeit with varying degrees of dominance in each distribution. As the ratio of the instantaneous value of the relaxation function (β^G) increases, the decline in displacements follows a descending order $(XD,\ UD,\ VD,\ OD)$ for carbon nanotube distributions. Conversely, the effect of the volume fraction of carbon nanotube on displacements differs across distributions, listed in descending order (XD, UD, VD, OD). It is seen that an increase in both coefficients enhances their respective effects, further reducing displacements.

In the last part of the study, a maximum of displacement study is carried out for simply supported FG-CNTRC viscoelastic plate with the material and geometric properties used in the first example of forced vibration analysis. The coefficient of carbon nanotube is taken as 0.11. Also, m and n are taken as 1. Maximum displacements vary depending on various carbon nanotube distributions $(UD,\ VD,\ XD,\ OD)$, the ratios of instantaneous value (β^G) and retardation times of the relaxation function $(\tau_r^G \times 10^{-5})$. In the given graphs, there are β^G on the horizontal axis. Each curve represents different τ_r^G and each graph shows different carbon nanotube distribution.

It is clearly seen from Fig. 9 that the displacements calculated according to carbon nanotube distributions are listed in descending order such as $w_{OD},\ w_{VD},\ w_{UD},\ w_{XD}$. As both τ_r^G and β^G increase, displacements decrease. The increase in these two viscoelastic parameters increases the effect of each other. The decrease in displacements as β^G and τ_r^G increase is listed in descending order such as XD, UD, VD, OD according to the distribution of carbon. The distance of each curve in the graphs to each other are listed in descending order such as $d_{OD},\ d_{VD},\ d_{UD},\ d_{XD}$, according to carbon nanotube distribution. It can be seen that the lowest displacements occur at the highest the ratio of instantaneous value and retardation time of the relaxation function in XD carbon nanotube distribution.

4. Conclusions

This study investigated the behavior of a simply supported FG-CNTRC viscoelastic plate under dynamic loads through free and forced vibration analyses, utilizing a linear viscoelastic model. Higher order shear deformation theory (HSDT) was applied to derive the displacement fields. Employing Hamilton's principle, equations of motion were acquired in the Laplace domain and later translated into the time domain via Durbin's modified inverse Laplace transform algorithm. A code was developed using Mathematica for the dynamic analysis of the simply supported FG-CNTRC viscoelastic plate. To validate the accuracy of this code, a free vibration analysis was conducted and compared against established literature. Subsequently, a forced vibration analysis was performed, leading to the following conclusions:

• An increase in the volume fraction of carbon nanotubes augments the material's Young's modulus, thereby boosting stiffness and reducing both displacements and periods.

• Based on the carbon nanotube distribution, the hierarchy of displacements and periods follows a descending order: $OD,\ VD,\ UD,\ XD$.

• Increasing β^G and τ_r^G leads to decreased displacements, yet these coefficients exhibit negligible impact on periods. Moreover, an elevated volume fraction of carbon nanotube diminishes the effects of β^G and τ_r^G. In essence, as V_{CNT}^* increases, the reduction in displacements due to β^G and τ_r^G diminishes.

• The influence of β^G and τ_r^G, and V_{CNT}^* coefficients on displacement and periods remains consistent across all carbon nanotube distributions.

However, the dominance of these effects on displacements varies across distributions. The carbon nanotube distributions escalating the influence of β^G and τ_r^G, and V_{CNT}^* coefficients are ranked $as\ XD,\ UD,\ VD$ and OD, respectively.

• Examination of the graphs reveals that the lowest displacements occur within the XD carbon nanotube distribution, particularly at the highest ratio of the instantaneous value and retardation time of the relaxation function.

References

Akavci, S.S. (2014), "An efficient shear deformation theory for free vibration of functionally graded thick rectangular plates on elastic foundation" *Compos. Struct.*, **108**, 667–676. https://doi.org/10.1016/j.compstruct.2013.10.019

Alibeigloo, A. and Emtehani, A. (2015), "Static and free vibration analyses of carbon nanotube-reinforced composite plate using differential quadrature method", *Meccanica*, **50**(1), 61-76. https://doi.org/10.1007/s11012-014-0050-7

Ansari, R., Hasrati, E., Faghih Shojaei, M., Gholami, R. and Shahabodini, A. (2015), "Forced vibration analysis of functionally graded carbon nanotube-reinforced composite plates using a numerical strategy", *Physica E*, **69**, 294-305. https://doi.org/10.1016/j.physe.2015.01.011

Ansari, R., Torabi, J. and Hosein Shakouri, A. (2017), "Vibration analysis of functionally graded carbon nanotube-reinforced composite elliptical plates using a numerical strategy", *Aerosp. Sci. Technol.*, **60**, 152-161. https://doi.org/10.1016/j.ast.2016.11.004

Barati, M.R. and Zenkour, A.M. (2019), "Vibration analysis of functionally graded graphene platelet reinforced cylindrical shells with different porosity distributions", *Mech. Adv. Mater. Struct.*, **26**(18), 1580-1588. https://doi.org/10.1080/15376494.2018.1444235

Bendaho, B., Belabed, Z., Bourada, M., Benatta, M.A., Bourada, F. and Tounsi, A. (2019), "Assessment of new 2D and quasi-3D Nonlocal theories for free vibration analysis of size-dependent functionally graded (FG) nanoplates", *Adv. Nano Res.*, **7**(4), 277-292. https://doi.org/10.12989/anr.2019.7.4.277

Bennoun, M., Houari, M.S.A. and Tounsi, A. (2016), "A novel five-variable refined plate theory for vibration analysis of functionally graded sandwich plates", *Mech. Adv. Mater. Struct.*, **23**(4), 423-431. https://doi.org/10.1080/15376494.2014.984088

Boley, B.A. and Weiner, J.H. (1960), *Theory of Thermal Stresses*, John Wiley and Sons, Ltd.

Boutaleb, S., Benrahou, K.H., Bakora, A., Algarni, A., Bousahla, A.A., Tounsi, A., Tounsi, A. and Mahmoud, S.R. (2019), "Dynamic analysis of nanosize FG rectangular plates based on simple nonlocal quasi 3D HSDT", *Adv. Nano Res.*, **7**(3), 191. https://doi.org/10.12989/anr.2019.7.3.191

Cadek, M., Coleman, J.N., Barron, V., Hedicke, K. and Blau, W.J. (2002), "Morphological and mechanical properties of carbon-nanotube-reinforced semicrystalline and amorphous polymer composites", *App. Phys. Lett.*, **81**(27), 5123-5125. https://doi.org/10.1063/1.1533118

Calim, F.F. (2003), "Dynamic analysis of viscoelastic, anisotropic curved spatial rod systems", Ph. D. Dissertation, Cukurova University, Adana, Turkey. (In Turkish)

Calim, F.F. (2016), "Dynamic response of curved Timoshenko beams resting on viscoelastic foundation", *Struct. Eng. Mech.*, **59**(4), 761-774. https://doi.org/10.12989/sem.2016.59.4.761

Calim, F.F. (2020), "Vibration analysis of functionally graded Timoshenko beams on Winkler-Pasternak elastic foundation", *Iran. J. Sci. Technol. Trans. Civ. Eng.*, **44**(3), 901-920. https://doi.org/10.1007/s40996-019-00283-x

Calim, F.F. and Cuma, Y.C. (2022), "Vibration analysis of nonuniform hyperboloidal and barrel helices made of functionally graded material", *Mech. Based Des. Struct.*, **50**(11), 3781-3795. https://doi.org/10.1080/15397734.2020.1822181

Calim, F.F. and Cuma, Y.C. (2023), "Forced vibration analysis of viscoelastic helical rods with varying cross-section and functionally graded material", *Mech. Based Des. Struct.*, **51**(7), 3620-3631. https://doi.org/10.1080/15397734.2021.1931307

Calim, F.F. and Özbey, M.B. (2024), "Damped response of porous functionally graded viscoelastic cylindrical shells", *Mech. Based Des. Struct.*, 1-20. https://doi.org/10.1080/15397734.2023.2242482

Cuma, Y.C. and Calim, F.F. (2021a), "Free vibration analysis of functionally graded cylindrical helices with variable cross-section", *J. Sound Vib.*, **494**, 115856. https://doi.org/10.1016/j.jsv.2020.115856

Cuma, Y.C. and Calim, F.F. (2021b), "Transient response of functionally graded non-uniform cylindrical helical rods", *Steel Compos. Struct.*, **40**(4), 571-580. https://doi.org/10.12989/scs.2021.40.4.571

Cuma, Y.C. and Calim, F.F. (2022), "Dynamic response of viscoelastic functionally graded barrel and hyperboloidal coil springs with variable cross-sectional area", *Mech. Time-Depend. Mater.*, **26**(4), 923-937. https://doi.org/10.1007/s11043-021-09520-1

Cuma, Y.C., Özbey, M.B. and Calim, F.F. (2024), "Vibration and damping analysis of functionally graded shells", *Mech. Time-*

Depend. Mater., 1-24. https://doi.org/10.1007/s11043-023-09621-z

Dang, X.H., Nguyen, V.L., Tran, M.T. and Nguyen Thi, B.P. (2022), "Free vibration characteristics of rotating functionally graded porous circular cylindrical shells with different boundary conditions", *IJST-T Mech. Eng.*, **46**(1), 167-183. https://doi.org/10.1007/s40997-020-00413-1

Duc, N.D. and Quan, T.Q. (2014), "Transient responses of functionally graded double curved shallow shells with temperature-dependent material properties in thermal environment", *Eur. J. Mech. A, Solids*, **47**, 101-123. https://doi.org/10.1016/j.euromechsol.2014.03.002

Durbin, F. (1974), "Numerical inversion of laplace transforms: an efficient improvement to Dubner and Abate's method", *Comput. J.*, **17**(4), 371-376. https://doi.org/10.1093/comjnl/17.4.371

Ebrahimi, F. and Farazmandnia, N. (2017), "Thermo-mechanical vibration analysis of sandwich beams with functionally graded carbon nanotube-reinforced composite face sheets based on a higher-order shear deformation beam theory", *Mech. Adv. Mater. Struct.*, **24**(10), 820-829. https://doi.org/10.1080/15376494.2016.1196786

Ebrahimi, F. and Habibi, S. (2017), "Low-velocity impact response of laminated FG-CNT reinforced composite plates in thermal environment" *Adv. Nano Res.*, **5**(2), 69. https://doi.org/10.12989/anr.2017.5.2.069

Emdadi, M., Mohammadimehr, M. and Navi, B.R. (2019), "Free vibration of an annular sandwich plate with CNTRC facesheets and FG porous cores using Ritz method", *Adv. Nano Res*, **7**(2), 109. https://doi.org/10.12989/anr.2019.7.2.109

Eratlı, N., Argeso, H., Calim, F.F., Temel, B. and Omurtag, M.H. (2014), "Dynamic analysis of linear viscoelastic cylindrical and conical helicoidal rods using the mixed FEM," *J. Sound Vib.* **333**, 3671-3690. https://doi.org/10.1016/j.jsv.2014.03.017

Faleh, N.M., Fenjan, R.M. and Ahmed, R.A. (2020), "Forced vibrations of multi-phase crystalline porous shells based on strain gradient elasticity and pulse load effects", *J. Vib. Eng. Technol.*, **8**(6), 925-933. https://doi.org/10.1007/s42417-020-00203-8

Fiedler, B., Gojny, F.H., Wichmann, M.H.G., Nolte, M.C.M. and Schulte, K. (2006), "Fundamental aspects of nano-reinforced composites", *Compos. Sci. Technol.*, **66**(16), 3115-3125. https://doi.org/10.1016/j.compscitech.2005.01.014

Ghasemi, A.R. and Mohandes, M. (2020), "Free vibration analysis of micro and nano fiber-metal laminates circular cylindrical shells based on modified couple stress theory", *Mech. Adv. Mater. Struct.*, **27**(1), 43-54. https://doi.org/10.1080/15376494.2018.1472337

Hajmohammad, M.H., Zarei, M.S., Nouri, A. and Kolahchi, R. (2017), "Dynamic buckling of sensor/functionally graded-carbon nanotube-reinforced laminated plates/actuator based on sinusoidal-visco-piezoelasticity theories", *J. Sandw. Struct. Mater.*, 1099636217720373. https://doi.org/10.1177/1099636217720373

Huang, B., Guo, Y., Wang, J., Du, J., Qian, Z., Ma, T. and Yi, L. (2016), "Bending and free vibration analyses of anti-symmetrically laminated carbon nanotube-reinforced functionally graded plates", *J. Compos. Mater.*, **51**(22), 3111-3125. https://doi.org/10.1177/0021998316685165

Khosravi, F., Simyari, M., Hosseini, S.A. and Tounsi, A. (2020), "Size dependent axial free and forced vibration of carbon nanotube via different rod models", *Adv. Nano Res.*, **9**(3), 157. https://doi.org/10.12989/anr.2020.9.3.157

Khosravi, S., Arvin, H. and Kiani, Y. (2019), "Interactive thermal and inertial buckling of rotating temperature-dependent FG-CNT reinforced composite beams", *Compos. Part B Eng.*, **175**, 107178. https://doi.org/10.1016/j.compositesb.2019.107178

Kiani, Y. (2017), "Analysis of FG-CNT reinforced composite conical panel subjected to moving load using Ritz method", *Thin Wall. Struct.*, **119**, 47-57. https://doi.org/10.1016/j.tws.2017.05.031

Kiani, Y. (2017), "Buckling of FG-CNT-reinforced composite plates subjected to parabolic loading", *Acta. Mech.*, **228**, 1303-1319. https://doi.org/10.1007/s00707-016-1781-4

Kiani, Y. (2017), "Dynamics of FG-CNT reinforced composite cylindrical panel subjected to moving load", *Thin Wall. Struct.*, **111**, 48-57. https://doi.org/10.1016/j.tws.2016.11.011

Kiani, Y. (2017), "Free vibration of FG-CNT reinforced composite spherical shell panels using Gram-Schmidt shape functions", *Compos. Struct.*, **159**, 368-381. https://doi.org/10.1016/j.compstruct.2016.09.079

Kim, Y.W. (2015), "Free vibration analysis of FGM cylindrical shell partially resting on Pasternak elastic foundation with an oblique edge", *Compos. Part B Eng.*, **70**, 263-276. https://doi.org/10.1016/j.compositesb.2014.11.024

Lei, Z.X., Liew, K.M. and Yu, J.L. (2013), "Free vibration analysis of functionally graded carbon nanotube-reinforced composite plates using the element-free kp-Ritz method in thermal environment", *Compos. Struct.*, **106**, 128-138. https://doi.org/10.1016/j.compstruct.2013.06.003

Lin, F. and Xiang, Y. (2014), "Vibration analysis of carbon nanotube reinforced composite plates", *Appl. Mech. Mater.*, **553**, 681-686. https://doi.org/10.4028/www.scientific.net/AMM.553.681

Liu, Y., Qin, Z. and Chu, F. (2021), "Nonlinear forced vibrations of FGM sandwich cylindrical shells with porosities on an elastic substrate", *Nonlinear Dyn.*, **104**(2), 1007-1021. https://doi.org/10.1007/s11071-021-06358-7

Mahapatra, T.R., Panda, S.K. and Kar, V.R. (2016), "Nonlinear hygro-thermo-elastic vibration analysis of doubly curved composite shell panel using finite element micromechanical model", *Mech. Adv. Mater. Struct.*, **23**(11), 1343-1359. https://doi.org/10.1080/15376494.2015.1085606

Malekzadeh, P. and Heydarpour, Y. (2015), "Mixed Navier-layerwise differential quadrature three-dimensional static and free vibration analysis of functionally graded carbon nanotube reinforced composite laminated plates", *Meccanica*, **50**(1), 143-167. https://doi.org/10.1007/s11012-014-0061-4

Mirjavadi, S.S., Forsat, M., Barati, M.R. and Hamouda, A.M.S. (2022), "Geometrically nonlinear vibration analysis of eccentrically stiffened porous functionally graded annular spherical shell segments", *Mech. Based Des. Struct.*, **50**(6), 2206-2220. https://doi.org/10.1080/15397734.2020.1771729

Mirzaei, M., Kiani, Y. (2015), "Snap-through phenomenon in a thermally postbuckled temperature dependent sandwich beam with FG-CNTRC face sheets", *Compos. Struct.*, **134**, 1004-1013. https://doi.org/10.1016/j.compstruct.2015.09.003

Mirzaei, M., Kiani, Y. (2016), "Free vibration of functionally graded carbon-nanotube-reinforced composite plates with cutout", *Beilstein J. Nanotechnol.*, **7**, 511-523. https://doi.org/10.3762/bjnano.7.45

Narayanan, G. V. (1980), "Numerical operational methods in structural dynamics", University of Minnesota, U.S.A.

Phung-Van, P., Abdel-Wahab, M., Liew, K.M., Bordas, S.P.A. and Nguyen-Xuan, H. (2015), "Isogeometric analysis of functionally graded carbon nanotube-reinforced composite plates using higher-order shear deformation theory", *Compos. Struct.*, **123**, 137-149. https://doi.org/10.1016/j.compstruct.2014.12.021

Rachid, A., Ouinas, D., Lousdad, A., Zaoui, F.Z., Achour, B., Gasmi, H., Butt, T.A. and Tounsi, A. (2022), "Mechanical behavior and free vibration analysis of FG doubly curved shells on elastic foundation via a new modified displacements field model of 2D and quasi-3D HSDTs", *Thin Wall. Struct.*, **172**,

108783. https://doi.org/10.1016/j.tws.2021.108783
Singha, T.D., Bandyopadhyay, T. and Karmakar, A. (2022), "A numerical solution for thermal free vibration analysis of rotating pre-twisted FG-GRC cylindrical shell panel", *Mech. Adv. Mater. Struct.*, 1-19. https://doi.org/10.1080/15376494.2022.2067924
Soleimani-Javid, Z., Arshid, E., Khorasani, M., Amir, S. and Tounsi, A. (2021), "Size-dependent flexoelectricity-based vibration characteristics of honeycomb sandwich plates with various boundary conditions", *Adv. Nano Res.*, **10**(5), 449-460. https://doi.org/10.12989/anr.2021.10.5.449
Temel, B., Calim, F.F. and Tütüncü, N. (2004), "Quasi-static and dynamic response of viscoelastic helical rods", *J. Sound Vib.*, **271**(3), 921-935. https://doi.org/10.1016/S0022-460X(03)00760-0
Thostenson, E.T., Ren, Z. and Chou, T.W. (2001), "Advances in the science and technology of carbon nanotubes and their composites: A review", *Compos. Sci. Technol.*, **61**(13), 1899-1912. https://doi.org/10.1016/S0266-3538(01)00094-X
Truong-Thi, T., Vo-Duy, T., Ho-Huu, V. and Nguyen-Thoi, T. (2020), "Static and free vibration analyses of functionally graded carbon nanotube reinforced composite plates using CS-DSG3", *Int. J. Comput. Methods*, **17**(03), 1850133. https://doi.org/10.1142/S021987621850133
Turker, H.T., Cuma, Y.C. and Calim, F.F. (2023), "An efficient approach for free vibration behaviour of non-uniform and non-homogeneous helices", *IJST-T Civ. Eng.*, **47**(4), 1959-1970. https://doi.org/10.1007/s40996-023-01075-0
Van Vinh, P. and Tounsi, A. (2022), "Free vibration analysis of functionally graded doubly curved nanoshells using nonlocal first-order shear deformation theory with variable nonlocal parameters", *Thin Wall. Struct.*, **174**, 109084. https://doi.org/10.1016/j.tws.2022.109084
Wang, M., Li, Z.M. and Qiao, P. (2016), "Semi-analytical solutions to buckling and free vibration analysis of carbon nanotube-reinforced composite thin plates", *Compos. Struct.*, **144**, 33-43. https://doi.org/10.1016/j.compstruct.2016.02.025
Wang, M., Li, Z.M. and Qiao, P. (2018), "Vibration analysis of sandwich plates with carbon nanotube-reinforced composite face-sheets", *Compos. Struct.*, **200**, 799-809. https://doi.org/10.1016/j.compstruct.2018.05.058
Wang, Q., Cui, X., Qin, B. and Liang, Q. (2017), "Vibration analysis of the functionally graded carbon nanotube reinforced composite shallow shells with arbitrary boundary conditions", *Compos. Struct.*, **182**, 364-379. https://doi.org/10.1016/j.compstruct.2017.09.043
Zannon, M., Abu-Rqayiq, A. and Al-bdour, A. (2020), "Free vibration frequency of thick FGM spherical shells based on a third-order shear deformation theory", *Eur. J. Pure Appl. Math.*, **13**(4), 766-778. https://doi.org/10.29020/nybg.ejpam.v13i4.3826
Zhang, Y., Guo, Z., Gong, Y., Shi, J., El Ouni, M.H. and Alhosny, F. (2023), "Elastic buckling performance of FG porous plates embedded between CNTRC piezoelectric patches based on a novel quasi 3D-HSDT in hygrothermal environment", *Adv. Nano Res.*, **15**(2), 175-189. https://doi.org/10.12989/anr.2023.15.2.175
Zhu, P., Lei, Z.X. and Liew, K.M. (2012), "Static and free vibration analyses of carbon nanotube-reinforced composite plates using finite element method with first order shear deformation plate theory", *Compos. Struct.*, **94**(4), 1450-1460. https://doi.org/10.1016/j.compstruct.2011.11.010

Appendix A

$$\alpha = m\pi/a,\ \beta = n\pi/b \tag{A.1}$$

$$k_{11} = A_{11}\alpha^2 + A_{66}\beta^2 \tag{A.2}$$

$$k_{12} = k_{21} = \alpha\beta(A_{12} + A_{66}) \tag{A.3}$$

$$k_{13} = k_{31} = -B_{11}\,\alpha^3 - \alpha\beta^2(B_{12} + 2B_{66}) \tag{A.4}$$

$$k_{14} = k_{41} = C_{11}\alpha^2 + C_{66}\beta^2 \tag{A.5}$$

$$k_{15} = k_{51} = \alpha\beta\,(C_{12} + C_{66}) \tag{A.6}$$

$$k_{22} = A_{66}\alpha^2 + A_{22}\beta^2 \tag{A.7}$$

$$k_{23} = k_{32} = -B_{22}\,\beta^3 - \beta\alpha^2(B_{12} + 2B_{66}) \tag{A.8}$$

$$k_{24} = k_{42} = \alpha\beta\,(C_{12} + C_{66}) \tag{A.9}$$

$$k_{25} = k_{52} = C_{66}\alpha^2 + C_{22}\beta^2 \tag{A.10}$$

$$k_{33} = D_{11}\alpha^4 + 2D_{12}\alpha^2\beta^2 + 4D_{66}\alpha^2\beta^2 + D_{22}\beta^4 \tag{A.11}$$

$$k_{34} = k_{43} = -E_{11}\alpha^3 - \alpha\beta^2(E_{12} + 2E_{66}) \tag{A.12}$$

$$k_{35} = k_{53} = -E_{22}\beta^3 - \beta\alpha^2(E_{12} + 2E_{66}) \tag{A.13}$$

$$\mathrm{k}_{44} = F_{55} + G_{11}\alpha^2 + G_{66}\beta^2 \tag{A.14}$$

$$\mathrm{k}_{45} = \mathrm{k}_{54} = \alpha\beta\,(G_{12} + G_{66}) \tag{A.15}$$

$$\mathrm{k}_{55} = F_{44} + G_{66}\alpha^2 + G_{22}\beta^2 \tag{A.16}$$

$$m_{11} = \mathrm{I}_1 \tag{A.17}$$

$$\mathrm{m}_{12} = m_{21} = m_{15} = \mathrm{m}_{51} = m_{24} = \mathrm{m}_{42} = m_{45} = m_{54} = 0 \tag{A.18}$$

$$m_{13} = m_{31} = -\mathrm{I}_2\alpha \tag{A.19}$$

$$m_{14} = m_{41} = \mathrm{I}_4 \tag{A.20}$$

$$m_{22} = \mathrm{I}_1 \tag{A.21}$$

$$\mathrm{m}_{23} = m_{32} = -\mathrm{I}_2\beta \tag{A.22}$$

$$\mathrm{m}_{25} = m_{52} = \mathrm{I}_4 \tag{A.23}$$

$$\mathrm{m}_{33} = \mathrm{I}_1 + \mathrm{I}_3(\alpha^2 + \beta^2) \tag{A.24}$$

$$\mathrm{m}_{34} = \mathrm{m}_{43} = -\mathrm{I}_5\alpha \tag{A.25}$$

$$\mathrm{m}_{35} = \mathrm{m}_{53} = -\mathrm{I}_5\beta \tag{A.26}$$

$$\mathrm{m}_{44} = \mathrm{m}_{55} = \mathrm{I}_6 \tag{A.27}$$

Appendix B

Displacements obtained in Laplace domain are converted to time domain using Durbin's modified inverse Laplace transform method, as shown below.

$$f(t_j) \cong \frac{2\, e^{a j \Delta t}}{T}\left[-\frac{1}{2} Re\{\bar{F}(a)\} + Re\left\{\sum_{k=0}^{N-1}\{\bar{F}(p_k)\, L_k\, e^{i\left(\frac{2\pi}{N}\right) j\, k}\right\}\right] \quad \text{(B.1)}$$

$$L_k = 1\ for\ k = 0\ ,\ L_k = \frac{sin\left(\frac{k\pi}{N}\right)}{\frac{k\pi}{N}}\ for\ k > 0 \quad \text{(B.2)}$$

here, $\boldsymbol{i}$ is complex number, $\boldsymbol{L_k}$ is Lanczos factor, $\boldsymbol{N}$ is the number of solution steps and $\boldsymbol{p_k}$ is Laplace transformation parameter. The calculation of $\boldsymbol{p_k}$ is carried out with $\boldsymbol{a + i\frac{2\pi k}{T}}$. Here $\boldsymbol{T}$ the total solution time. The $\boldsymbol{t_j}$ calculation used in calculating $\boldsymbol{f(t_j)}$ is $\boldsymbol{t_j = j\Delta t = \frac{jT}{N}}$, $(\boldsymbol{j = 0, 1, 2, \ldots, N-1})$. While $\boldsymbol{aT}$ is a value between 5 and 10, it is observed that its optimum value is 6 from previous studies.